NANO EXPRESS   **Open Access**

Efficient perovskite solar cells based on low-temperature solution-processed (CH$_3$NH$_3$)PbI$_3$ perovskite/CuInS$_2$ planar heterojunctions

Chong Chen[1,2*], Chunxi Li[1,2], Fumin Li[1,2*], Fan Wu[3], Furui Tan[1,2], Yong Zhai[1,2] and Weifeng Zhang[1,2]

Abstract

In this work, the solution-processed CH$_3$NH$_3$PbI$_3$ perovskite/copper indium disulfide (CuInS$_2$) planar heterojunction solar cells with Al$_2$O$_3$ as a scaffold were fabricated at a temperature as low as 250°C for the first time, in which the indium tin oxide (ITO)-coated glass instead of the fluorine-doped tin oxide (FTO)-coated glass was used as the light-incidence electrode and the solution-processed CuInS$_2$ layer was prepared to replace the commonly used TiO$_2$ layer in previously reported perovskite-based solar cells. The influence of the thickness of the as-prepared CuInS$_2$ film on the performance of the ITO/CuInS$_2$(n)/Al$_2$O$_3$/(CH$_3$NH$_3$)PbI$_3$/Ag cells was investigated. The ITO/CuInS$_2$(2)/ Al$_2$O$_3$/(CH$_3$NH$_3$)PbI$_3$/Ag cell showed the best performance and achieved power conversion efficiency up to 5.30%.

Keywords: Solution-processed; Solar cells; (CH$_3$NH$_3$)PbI$_3$; Perovskite; CuInS$_2$

Background

Thin-film solar cells have attracted considerable attention because of simplified and low-cost fabrication procedures compared to conventional silicon-based solar cells. The thin-film solar cells based on inorganic photovoltaic materials processed with expensive vacuum-based techniques and/or high-temperature sintering exhibit high efficiency [1-3]. However, the use of these thin-film solar cells is still limited because the manufacturing costs are still relatively high. To lower the cost of device fabrication, the low-temperature solution-based techniques such as spin coating and chemical bath deposition are needed to prepare inorganic photovoltaic materials. The thin-film solar cells based on the solution-processed inorganic nanocrystals such as PbS [4,5], CdTe [6,7], CdSe [8], copper indium disulfide (CuInS$_2$) [9,10], and Cu$_2$ZnSnS$_4$ [11] have been demonstrated, but their maximum solar power conversion efficiency is still low. The main reason for the low efficiency is that the low-temperature solution-processed inorganic nanocrystals are typically amorphous or poorly crystalline, leading to poor charge carrier transport because of short carrier diffusion lengths (typically about

10 nm). Therefore, the new solution-based techniques to improve the crystalline structures of inorganic nanocrystals are needed. For example, to enhance the carrier transport in CuInS$_2$, a method of using a molecular-based precursor solution has been presented [10] to synthesize CuInS$_2$ nanocrystals with a polycrystalline structure at relatively lower temperatures (<250°C) for the solution-processed inorganic solar cells. Besides, the inorganic materials which can be processed with solution-based techniques and generated charge carriers with long diffusion lengths in the bulk are sought.

The recently reported semiconducting perovskite materials such as (CH$_3$NH$_3$)PbX$_3$ (X = Cl, Br, I) could fulfil these requirements. These perovskites have high charge carrier mobilities and long charge carrier lifetime, which means that the light-generated charges have long carrier transport lengths [12]. It has been reported that the effective diffusion lengths are about 100 nm for both electrons and holes [13,14]. In addition, these perovskites with a direct bandgap have a broad range of light absorption and high extinction coefficient [15,16]. Due to their super electrical properties and super light-harvesting characteristics, the perovskites have been used in a variety of nanostructured solar cells and have achieved high-power conversion efficiencies (>9%) [16-20]. In solid-state sensitized solar cells, the CH$_3$NH$_3$PbI$_3$ used as the sensitizer

* Correspondence: mrchenchong@163.com; lfm0613@gmail.com
[1]School of Physics and Electronics, Henan University, Kaifeng 475004, People's Republic of China
Full list of author information is available at the end of the article

has led to a high-power conversion efficiency of 15% [17]. The other perovskite-based nanostructured solar cells that commonly incorporated the perovskite as the absorbing layer between an n-type electron-transporting layer such as TiO_2 and a p-type hole-transporting layer such as 2,2′,7,7′-tetrakis(N, V-di-p-methoxyphenylamino)-9,9′-spirobifluorene (Spiro-OMeTAD) have also demonstrated high efficiencies [15,18,21]. Moreover, the research results reported by Lee et al.[16], Etgar et al.[22], and Ball et al. [23] showed that the perovskites have good charge (electron or hole)-transport properties, resulting in high efficiencies of the solar cells. Nevertheless, in these perovskite-based nanostructured solar cells, the transparent TiO_2 compact layer between the conducting substrate and perovskite materials or the scaffold (Al_2O_3) generally requires high-temperature sintering at about 500°C [15,17,18,23,24], which limits substrate choice and is incompatible with the low-cost solar technology. Therefore, the low-temperature solution-processed semiconductor materials that could replace the TiO_2 for the perovskite-based nanostructured solar cells are needed. In addition to the preparation method, the electronic energy levels (EELs) of those substitute materials are needed to match the EELs of the perovskite materials for efficient charge transfer. For this purpose, ZnO compact layer and ZnO nanorods are recently prepared by electrodeposition and chemical bath deposition, respectively, to replace the TiO_2 by Kumar et al. [25]. It is worth noting that the materials used to replace the TiO_2 do not necessarily have to be the n-type semiconductors such as the ZnO because the perovskites can conduct not only positive holes [22,26] but also electrons [16].

It is known that $CuInS_2$ as a p-type semiconductor is a very promising light-absorbing material for its direct bandgap of 1.5 eV, which is closely matched to the best bandgap (1.45 eV) of the solar cell materials [27]. Recently, a method of using a molecular-based precursor solution to synthesize $CuInS_2$ nanocrystals at relatively lower temperatures (250°C) has been presented by Li et al. [10]. More importantly, the valence band level (−5.6 eV) of the $CuInS_2$ is also matched to that (−5.6 or −6.5 eV) [13] of the $(CH_3NH_3)PbI_3$, which is very beneficial to the hole transfer from the $(CH_3NH_3)PbI_3$ to the $CuInS_2$. Therefore, replacing the TiO_2 with $CuInS_2$ is reasonable. In this study, for the first time, the p-type semiconductor material, $CuInS_2$, as both the light harvester and hole transporter is prepared by the reported method [10] to replace the commonly used n-type TiO_2 in the perovskite-based solar cells. Moreover, the indium tin oxide (ITO) glass rather than the commonly used fluorine-doped tin oxide (FTO) glass in previously reported perovskite-based solar cells is used as a light-incidence electrode because the $CuInS_2$ film can directly be deposited on the ITO glass at a temperature as low

as 250°C. After the deposition of $CuInS_2$ film, the Al_2O_3 and $(CH_3NH_3)PbI_3$ are successively deposited on the $CuInS_2$ film to form the $CuInS_2/(CH_3NH_3)PbI_3$ planar heterojunction. The porous Al_2O_3 layer acts as a scaffold. Finally, an evaporated Ag top electrode was deposited on the $(CH_3NH_3)PbI_3$ at a pressure of 10^{-6} Torr to complete the device fabrication. The schematics and energy diagram of the prepared solar cells are shown in Figure 1a, b, respectively. The surface morphology, structure characterization, and optical property of the prepared $CuInS_2/(CH_3NH_3)PbI_3$ film are studied. Furthermore, the influence of the thickness of the $CuInS_2$ film on the power conversion efficiency of the fabricated $CuInS_2/(CH_3NH_3)PbI_3$ planar heterojunction solar cell is investigated.

Methods
Materials
Indium acetate (In(OAc)$_3$, 99.99%), copper iodode (CuI, 99.999%), thiourea (≥99.0%), 1-propionic acid (≥99.5%), γ-butyrolactone (≥99.0%), aluminum oxide (Al_2O_3, 20 wt.% in isopropanol), methylamine (40 wt.% in H_2O), hydroiodic acid (57 wt.% in water), diethyl ether, and PbI_2 (99.999%) were purchased from Sigma-Aldrich (St. Louis, MO, USA). All the reagents were used without further purification. Indium tin oxide-coated glass slides (ITO, ≤15 Ω/square, Wuhu Token Sci. Co., Ltd., China) were cleaned by successive ultrasonic treatment in deionized water, acetone, and isopropyl alcohol and then dried at 100°C for 10 min.

Synthesis of $CuInS_2$ nanocrystal film on ITO substrate
$CuInS_2$ nanocrystals were synthesized through a spin-coating method, which is similar to that reported by Li et al. [10]. Briefly, CuI (0.11 mmol), In(OAc)$_3$ (0.1 mmol), and thiourea (0.5 mmol) were dissolved in a mixture of 1-butylamine (0.6 mL) and 1-propionic acid (40 μL) under a nitrogen atmosphere in a glovebox (O_2 < 0.1 ppm, H_2O < 0.1 ppm). The mixture was shaken for 1 min, and after which, the obtained $CuInS_2$ precursor solution was then spin-cast onto the cleaned ITO substrates at 4,000 rpm for 30 s. Then, the obtained films were calcined at 150°C for 10 min and then heated to 250°C and held for 15 min
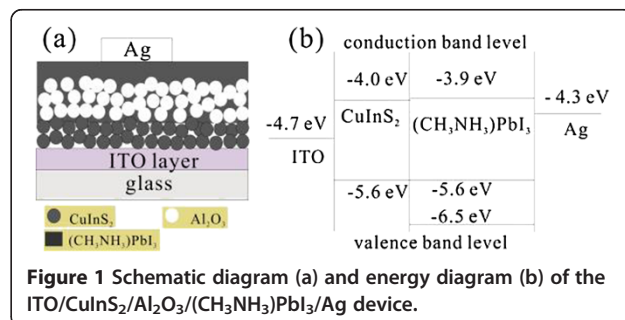

Figure 1 Schematic diagram (a) and energy diagram (b) of the ITO/CuInS$_2$/Al$_2$O$_3$/(CH$_3$NH$_3$)PbI$_3$/Ag device.

at this temperature. To change the thickness of the $CuInS_2$ film, a spinning-drying cycle was repeated several times. The $ITO/CuInS_2$ sample after n cycles of $CuInS_2$ deposition was denoted as $ITO/CuInS_2(n)$.

Synthesis of methylammonium iodide and $(CH_3NH_3)PbI_3$

Methylammonium iodide (CH_3NH_3I) was synthesized by reacting methylamine (aqueous, 40 wt.%) and hydroiodic acid (aqueous, 57 wt.%) in an ice bath for 2 h with stirring, as described elsewhere [18]. After that, the solvent was evaporated and the precipitate was washed using diethyl ether three times and dried at 60°C for 24 h in a vacuum oven. The resulting product, CH_3NH_3I, was used without further purification. To obtain a $(CH_3NH_3)PbI_3$ precursor, the synthesized CH_3NH_3I was mixed with PbI_2 at a 1:1 mol ratio in γ-butyrolactone (40% by weight) at 60°C.

Solar cell fabrication

First, a Al_2O_3 layer was introduced on the $ITO/CuInS_2(n)$ films by spin coating isopropanol solution containing Al_2O_3 nanoparticles at 4,000 rpm for 60 s. After that, the films were dried at 150°C for 30 min to obtain $ITO/CuInS_2(n)/Al_2O_3$. Then, the prepared $ITO/CuInS_2(n)/Al_2O_3$ films were spin-coated with the obtained $(CH_3NH_3)PbI_3$/γ-butyrolactone solution at 3,000 rpm for 60 s and then dried at 100°C for 1 h to form crystalline $(CH_3NH_3)PbI_3$. The prepared $ITO/CuInS_2(n)/Al_2O_3/(CH_3NH_3)PbI_3$ films were naturally cooled to room temperature. All the experiment was finished in a nitrogen glovebox ($O_2 < 0.1$ ppm, $H_2O < 0.1$ ppm). Finally, a silver back contact layer was deposited by thermal evaporation onto the $ITO/CuInS_2(n)/(CH_3NH_3)PbI_3$ films from a silver wire (99.999%).

Characterization

The surface morphology and structure of the prepared $ITO/CuInS_2(n)$ and $ITO/CuInS_2(n)/Al_2O_3/(CH_3NH_3)PbI_3$ films were characterized using a scanning electron microscope (SEM) (JSM-7001 F, Japan Electron Optics Laboratory Co., Ltd., Tokyo, Japan) and power X-ray diffractometry (XRD) (DX-2500, Dandong Fangyuan Instrument Co., Ltd., Dandong, China), respectively. It should be noted that, for XRD measurement, the $CuInS_2$ and $(CH_3NH_3)PbI_3$ films are individually deposited on the cleaned glass without ITO layer to exclude the influence of the substrate on the XRD measurement. UV-visible absorption measurements were conducted using a UV–vis spectrophotometer (UV-2550, Shimadzu Corporation, Kyoto, Japan). Current density-voltage (J-V) characteristics of the as-prepared solar cells were measured using a Keithley 2410 SourceMeter (Keithley Instruments, Inc., Cleveland, OH, USA). A solar simulator (Newport Inc., Irvine, CA, USA) was used as the light source to provide AM 1.5 G simulated solar light (100 mW/cm^2). Before each measurement, the light intensity was determined using a calibrated Si reference diode. For all measurements, the effective illumination area of the cells was 4 mm^2. The monochromatic incident photon-to-electron conversion efficiency (IPCE) spectra for the fabricated solar cells were measured using a commercial setup (QTest Station 2000 IPCE Measurement System, Crowntech, Macungie, PA, USA).

Results and discussion

The morphology, structures, and chemical composition of the as-prepared $CuInS_2$ were studied with SEM studies accompanied by energy dispersive X-ray spectrometry (EDX). Figure 2a shows a typical top-view SEM image of the $ITO/CuInS_2(1)$ film. As shown in Figure 2a, the surface of the ITO substrate is covered with the $CuInS_2$ film. The $CuInS_2$ film is composed of $CuInS_2$ nanoparticles, and these $CuInS_2$ nanoparticles appear to be fused together after heating at 250°C. Moreover, some voids can be clearly seen in the $ITO/CuInS_2$ (1) film, which can be explained by the decomposition of volatile surface ligands and precurse materials [10]. For a comparison, the SEM top image of the $ITO/CuInS_2(2)$ is displayed in Figure 2b. It can be observed that, compared to the $ITO/CuInS_2(1)$ film, the number of the voids in the $ITO/CuInS_2(2)$ film decreases significantly, indicating that the voids in the $ITO/CuInS_2(1)$ have been filled by the $CuInS_2$ precursor after two times of spin coating. In addition, the cross-sectional SEM images of the $ITO/CuInS_2(2)$, $ITO/CuInS_2(2)/Al_2O_3$, and $ITO/CuInS_2(2)/Al_2O_3/(CH_3NH_3)PbI_3/Ag$ films are shown in Figure 2c. It clearly shows that the $CuInS_2(2)$ film with an average thickness of 400 nm is formed on the ITO glass, and there are no obvious voids in the film. After the deposition of Al_2O_3, the thickness of the $ITO/CuInS_2(2)/Al_2O_3$ film increased. After the deposition of $(CH_3NH_3)PbI_3$, the thickness of the $ITO/CuInS_2(2)/Al_2O_3/(CH_3NH_3)PbI_3$ film further increased to about 650 nm. The more important thing is that the $(CH_3NH_3)PbI_3$ precursor solution permeated into the porous Al_2O_3 layer to form the $(CH_3NH_3)PbI_3$. The corresponding EDX spectrum of $ITO/CuInS_2$ (2) is shown in Figure 2d, which shows the film is mainly composed of copper (Cu), indium (In), and sulfur (S). The chemical compositional analysis reveals that the atomic ratio of Cu, In, and S is 25.33%, 24.9%, and 49.77%, respectively, close to 1:1:2, which confirms the formation of $CuInS_2$.

To characterize the crystal structure of the $CuInS_2$, a typical XRD pattern of the as-prepared $CuInS_2(3)$ film on a clean glass substrate is shown in Figure 3. The well-defined peaks can be referred to a tetragonal $CuInS_2$ (112), (204), (220), (116), and (312) (JCPDS file no. 85–1575), which is in agreement with the reported results [10,28,29].
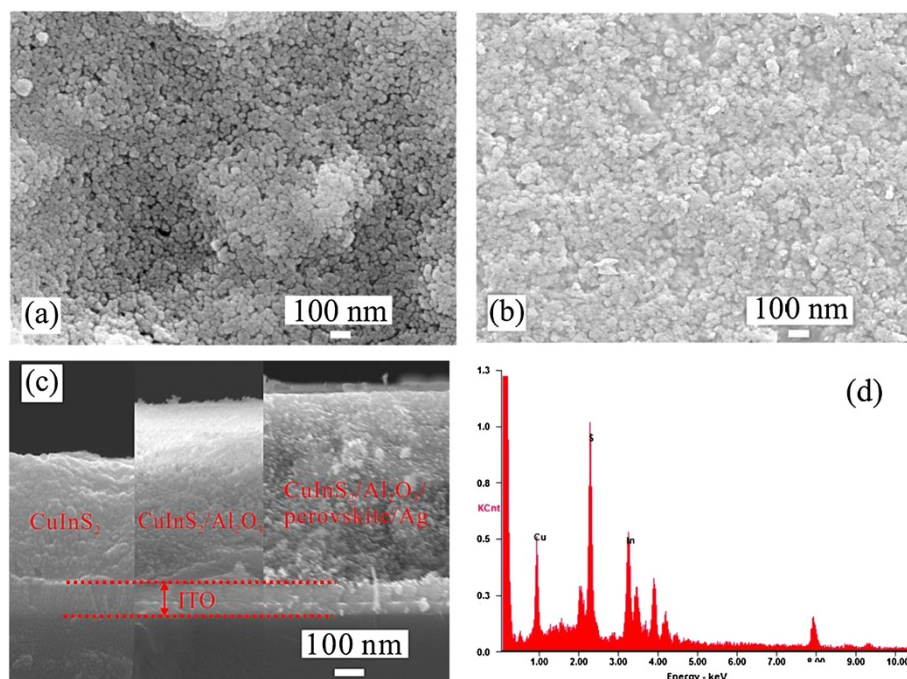
Figure 2 The morphology, structures, and chemical composition of the as-prepared CuInS$_2$. (a) Top view of the ITO/CuInS$_2$(1) film; **(b)** the top-view SEM image of the ITO/CuInS$_2$(2) film; **(c)** the cross-sectional images of the ITO/CuInS$_2$(2), ITO/CuInS$_2$(2)/Al$_2$O$_3$, and ITO/CuInS$_2$(2)/Al$_2$O$_3$/(CH$_3$NH$_3$)PbI$_3$/Ag films; and **(d)** the EDX spectrum of the ITO/CuInS$_2$(2) film.

Figure 4a shows a top-view SEM image of the ITO/CuInS$_2$(2)/Al$_2$O$_3$/(CH$_3$NH$_3$)PbI$_3$ film. By comparing this image with that (Figure 2b) of the ITO/CuInS$_2$(2) film, it can be clearly observed that the (CH$_3$NH$_3$)PbI$_3$ film was deposited on the CuInS$_2$. However, the solution-processed (CH$_3$NH$_3$)PbI$_3$ films are not very uniform and coated the CuInS$_2$ film only partially with micrometer-sized (CH$_3$NH$_3$)PbI$_3$ platelets, which is very similar to the observed phenomenon in the (CH$_3$NH$_3$)PbI$_3$-coved compact TiO$_2$ film [21]. Furthermore, to characterize the crystal structure and phase composition of the

Figure 3 The XRD pattern of the as-prepared CuInS$_2$(3) film.

synthesized (CH$_3$NH$_3$)PbI$_3$ film, the XRD analysis of the prepared (CH$_3$NH$_3$)PbI$_3$ film was performed and shown in Figure 4b. It can be seen from Figure 4b that the diffraction peaks are in good agreement with the tetragonal phase of the (CH$_3$NH$_3$) PbI$_3$ perovskite [17,30].

To study the light absorption properties of the prepared ITO/CuInS$_2$(n) and ITO/CuInS$_2$(n)/Al$_2$O$_3$/(CH$_3$NH$_3$)PbI$_3$ films for application in photovoltaic devices, light absorption studies are carried out. Figure 5 shows the UV–vis absorption spectra of the ITO/CuInS$_2$(1) and ITO/CuInS$_2$(n)/Al$_2$O$_3$/(CH$_3$NH$_3$)PbI$_3$ films (n = 1, 2, and 3). As shown in Figure 5, the ITO/CuInS$_2$(1) film has light absorption at wavelengths below 825 nm, which is similar to the reported results [10,31,32]. After the (CH$_3$NH$_3$)PbI$_3$ film was deposited on the ITO/CuInS$_2$(1) film, the absorbance of the spectra of the ITO/CuInS$_2$(1)/Al$_2$O$_3$/(CH$_3$NH$_3$)PbI$_3$ film increases significantly in the UV region as well as the visible region. For the ITO/CuInS$_2$(n)/Al$_2$O$_3$/(CH$_3$NH$_3$)PbI$_3$ films after other spin-cast cycles (n = 2 and 3) in our experiments, similar results are also obtained, which can be attributed to the light absorption of the deposited (CH$_3$NH$_3$)PbI$_3$ film. Moreover, for the ITO/CuInS$_2$(n)/Al$_2$O$_3$/(CH$_3$NH$_3$)PbI$_3$ films, Figure 5 also illustrates that the light absorbance was enhanced with an increase in spin-cast cycle number n, indicating an increased deposition amount of CuInS$_2$. In addition, the absorption lines of the ITO/CuInS$_2$/
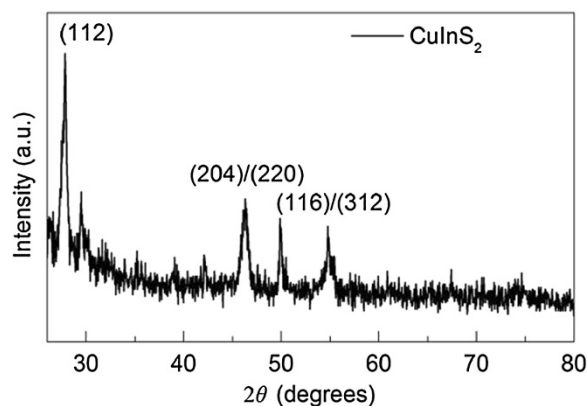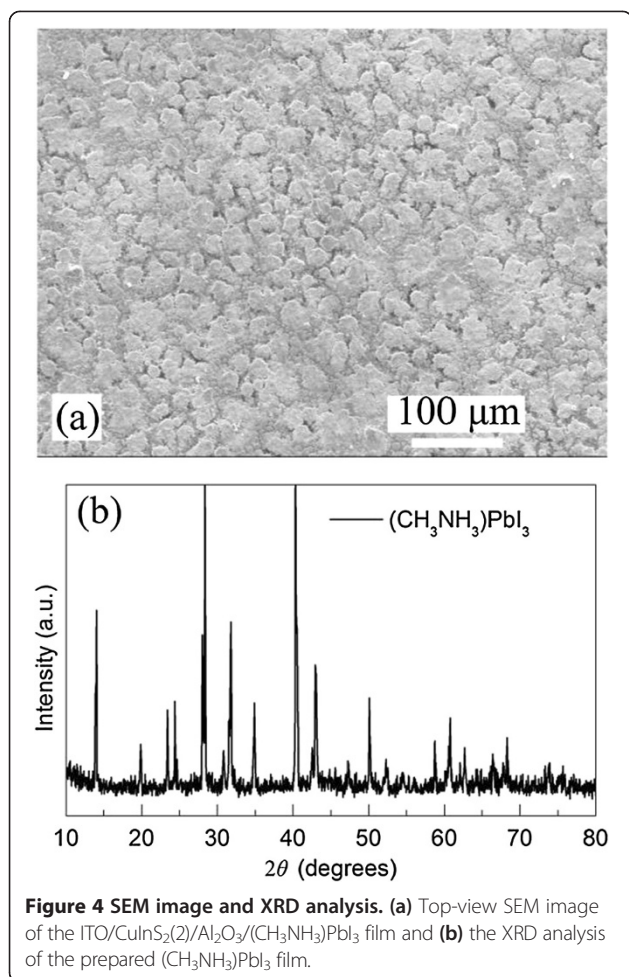
Figure 4 SEM image and XRD analysis. (a) Top-view SEM image of the ITO/CuInS$_2$(2)/Al$_2$O$_3$/(CH$_3$NH$_3$)PbI$_3$ film and **(b)** the XRD analysis of the prepared (CH$_3$NH$_3$)PbI$_3$ film.

(CH$_3$NH$_3$)PbI$_3$ films are very similar to those of the reported FTO/TiO$_2$/(CH$_3$NH$_3$)PbI$_3$ films [33], which further confirms the formation of (CH$_3$NH$_3$)PbI$_3$ film and shows the potential of the ITO/CuInS$_2$/Al$_2$O$_3$/(CH$_3$NH$_3$)PbI$_3$ films in photovoltaic application.
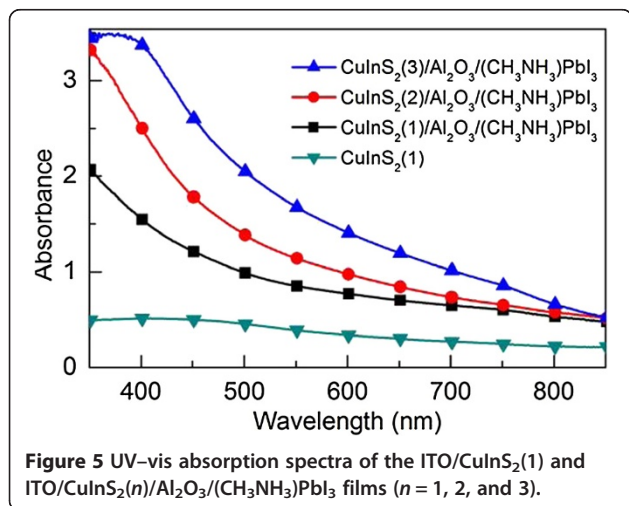
The *J-V* characteristics of the ITO/CuInS$_2$(*n*)/Al$_2$O$_3$/(CH$_3$NH$_3$)PbI$_3$/Ag solar cells under simulated AM 1.5 G solar irradiation and in the dark are shown in Figure 6. All device parameters under the light illumination, the open-circuit voltage (V_{oc}), the short-circuit photocurrent (J_{sc}), the fill factor (FF), and the solar power conversion efficiency (η), extracted from the *J-V* characteristics are summarized in Table 1. For the ITO/CuInS$_2$(*n*)/Al$_2$O$_3$/(CH$_3$NH$_3$)PbI$_3$/Ag cells, with the increase of CuInS$_2$ deposition number *n* from 1 to 2, the J_{sc} increased from 8.85 to 9.92 mA/cm^2, the V_{oc} increased from 0.74 to 0.76 V, the FF increased from 0.51 to 0.70, and the η increased from 3.31% to 5.30%. These results might be caused by the voids in the CuInS$_2$ film. As shown in Figure 2a, some voids have been found in the ITO/CuInS$_2$(1) film. When the (CH$_3$NH$_3$)PbI$_3$ precursor solution was spin-cast onto the ITO/CuInS$_2$(1)/Al$_2$O$_3$ film, these voids might be filled by the (CH$_3$NH$_3$)PbI$_3$ precursor solution. Therefore, similar to the observed phenomenon in the mesoporous-TiO$_2$/(CH$_3$NH$_3$)PbI$_3$ film, the (CH$_3$NH$_3$)PbI$_3$ probably infiltrated to the bottom of the CuInS$_2$ film and had a contact with the hole collection electrode (i.e., the ITO electrode), which will enhance the probability of recombination between electrons in the (CH$_3$NH$_3$)PbI$_3$ and holes in the ITO in the ITO/CuInS$_2$(1)/Al$_2$O$_3$/(CH$_3$NH$_3$)PbI$_3$/Ag solar cell. In contrast, as shown in Figure 2c, there are few voids in the ITO/CuInS$_2$(2) film, which may effectively reduce the charge recombination at the ITO/(CH$_3$NH$_3$)PbI$_3$ interface in the ITO/CuInS$_2$(2)/Al$_2$O$_3$/(CH$_3$NH$_3$)PbI$_3$/Ag solar cell. This explanation is supported by the *J-V* characteristics of the ITO/CuInS$_2$(*n*)/(CH$_3$NH$_3$)PbI$_3$/Ag in the dark (Figure 6) since the charge recombination can be typically represented by the dark current [2,34,35]. It can be observed that the dark current density of the ITO/CuInS$_2$(2)/Al$_2$O$_3$/(CH$_3$NH$_3$)PbI$_3$/Ag cell is lower than that of the ITO/CuInS$_2$(1)/

Figure 5 UV–vis absorption spectra of the ITO/CuInS$_2$(1) and ITO/CuInS$_2$(*n*)/Al$_2$O$_3$/(CH$_3$NH$_3$)PbI$_3$ films (*n* = 1, 2, and 3).

Figure 6 *J-V* characteristics. *J-V* characteristics of the ITO/CuInS$_2$ (*n*)/Al$_2$O$_3$/(CH$_3$NH$_3$)PbI$_3$/Ag solar cells under simulated AM 1.5G solar irradiation and in the dark (*n* = 1, 2, and 3).
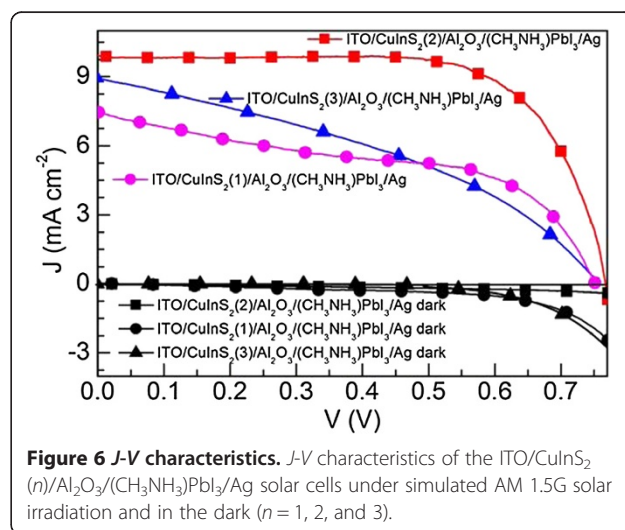
Table 1 Summary of device performance under white light illumination with an intensity of 100 mW/cm^2

Cells	V_{oc} (V)	J_{sc} (mA/cm^{-2})	FF	PCE (%)
ITO/CuInS$_2$(1)/Al$_2$O$_3$/ (CH$_3$NH$_3$)PbI$_3$/Ag	0.74	8.85	0.51	3.31
ITO/CuInS$_2$(2)/Al$_2$O$_3$/ (CH$_3$NH$_3$)PbI$_3$/Ag	0.76	9.92	0.70	5.30
ITO/CuInS$_2$(3)/Al$_2$O$_3$/ (CH$_3$NH$_3$)PbI$_3$/Ag	0.76	8.98	0.38	2.60

Al$_2$O$_3$/(CH$_3$NH$_3$)PbI$_3$/Ag cell, which indicates that the charge recombination is reduced in the ITO/CuInS$_2$(2)/ Al$_2$O$_3$/(CH$_3$NH$_3$)PbI$_3$/Ag cell.

However, the device performance of the ITO/CuInS$_2$ (n)/Al$_2$O$_3$/(CH$_3$NH$_3$)PbI$_3$/Ag cell decreased as the CuInS$_2$ deposition number n increased further from 2 to 3. It can be found from Table 1 that, compared to the ITO/CuInS$_2$ (2)/Al$_2$O$_3$/(CH$_3$NH$_3$) PbI$_3$/Ag cell, all device parameters (J_{sc}, FF, and η) except V_{oc} of the ITO/CuInS$_2$(3)/Al$_2$O$_3$/ (CH$_3$NH$_3$) PbI$_3$/Ag cell decreased. For the ITO/CuInS$_2$ (3)/Al$_2$O$_3$/(CH$_3$NH$_3$)PbI$_3$/Ag cell, the J_{sc}, FF, and η decreased to 8.98 mA/cm^2, 0.38, and 2.60%, respectively. The main reason for the decreased device performance may be the increased thickness of CuInS$_2$ film. As shown in Figure 1, in the ITO/CuInS$_2$/Al$_2$O$_3$/(CH$_3$NH$_3$)PbI$_3$/Ag cell, the CuInS$_2$ mainly conducted holes. Therefore, increasing the thickness of CuInS$_2$ film would increase the hole-transfer resistance and lead to an increase in overall series resistance (R_s) in the cells, which would inevitably lead to the degradation of J_{sc} and FF. The R_s can be calculated from the inverse slope of the illuminated J-V characteristics at $J = 0$. The R_s values for the ITO/CuInS$_2$ (2)/Al$_2$O$_3$/(CH$_3$NH$_3$)PbI$_3$/Ag and ITO/CuInS$_2$(3)/Al$_2$O$_3$/ (CH$_3$NH$_3$)PbI$_3$/Ag cells are 6.4 and 29.6 Ω/cm^2, respectively, which were calculated from the illuminated J-V characteristics (shown in Figure 6). Obviously, compared to the ITO/CuInS$_2$(2)/Al$_2$O$_3$/(CH$_3$NH$_3$)PbI$_3$/Ag cell, the R_s of ITO/CuInS$_2$(3)/Al$_2$O$_3$/(CH$_3$NH$_3$)PbI$_3$/Ag cell increased due to the increased thickness of the CuInS$_2$ film. Furthermore, a too thick CuInS$_2$ film may dramatically reduce the amount of light absorbed by the (CH$_3$NH$_3$)PbI$_3$ film, which results in a sizeable reduction in the number of the photo-generated electrons in the (CH$_3$NH$_3$)PbI$_3$ film and therefore reduces the J_{sc} and FF.

Figure 7 shows the IPCE spectra of the ITO/CuInS$_2$(2)/ Al$_2$O$_3$/(CH$_3$NH$_3$)PbI$_3$/Ag solar cell. It can be observed that the solar cell shows a spectral response in the almost entire wavelength region from 370 to 1,000 nm. The IPCE of over 31% is observed at a wavelength range from 370 to 750 nm. Furthermore, for the IPCE value, a sharp decrease in the wavelength region from 750 to 820 nm is observed. The threshold wavelength of 820 nm is related to the bandgap of about 1.5 eV for (CH$_3$NH$_3$)PbI$_3$ [36]. These results are in agreement with the previously reported IPCE
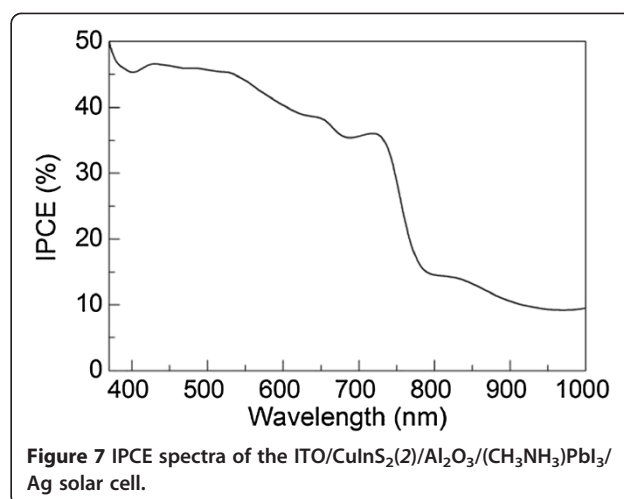

Figure 7 IPCE spectra of the ITO/CuInS$_2$(2)/Al$_2$O$_3$/(CH$_3$NH$_3$)PbI$_3$/ Ag solar cell.

spectra for the perovskite solar cells without a CuInS$_2$ layer [19,36,37]. It should be noted that, for these reported perovskite solar cells, the IPCE values are nearly zero in the long wavelength region (820 to 1,000 nm). However, in our case, IPCE of over 9% is observed at an entire wavelength range from 820 to 1,000 nm, resulting from the photocurrent originating from the CuInS$_2$ layer. Therefore, the CuInS$_2$ layer can improve the IPCE values of the solar cells in the long wavelength region.

Our experimental results demonstrated that, for the ITO/CuInS$_2$(n)/Al$_2$O$_3$/(CH$_3$NH$_3$)PbI$_3$/Ag cells, the ITO/ CuInS$_2$(2)/Al$_2$O$_3$/(CH$_3$NH$_3$)PbI$_3$/Ag cell showed the highest solar power conversion efficiency of 5.30%. However, it should be noted that the highest power conversion efficiency presented here was just taken from the solar cells with a simplified architecture. The solar cell architecture can be further optimized. For example, a hole-selective layer can be inserted between the ITO and the CuInS$_2$ layers to reduce the charge recombination at the ITO/ CuInS$_2$ interface. Similarly, inserting an electron-selective layer between the (CH$_3$NH$_3$)PbI$_3$ layer and the Ag electrode may also suppress the charge recombination at the (CH$_3$NH$_3$)PbI$_3$/Ag interface. Therefore, the solar cells with an architecture that incorporates the charge (hole or electron)-selective layer may achieve higher power conversion efficiency, which is our future study.

Conclusions

In summary, the solution-processed (CH$_3$NH$_3$)PbI$_3$ perovskite/CuInS$_2$ planar heterojunction solar cells with a Al$_2$O$_3$ scaffold have been successfully fabricated, in which the CuInS$_2$ films as both the light harvester and hole transporter were prepared at a relatively low temperature (250°C) via a simple solution-based chemical approach to replace the commonly used n-type TiO$_2$ layer. The influence of the thickness of CuInS$_2$ film on the performance of the fabricated ITO/CuInS$_2$/Al$_2$O$_3$/

(CH$_3$NH$_3$)PbI$_3$/Ag solar cells was investigated. Our experimental results demonstrated that an optimum power conversion efficiency of up to 5.30% can be achieved by the ITO/CuInS$_2$(2)/Al$_2$O$_3$/(CH$_3$NH$_3$)PbI$_3$/Ag cell. Optimizing the device architecture may further improve the performance of the ITO/CuInS$_2$(n)/Al$_2$O$_3$/(CH$_3$NH$_3$) PbI$_3$/Ag solar cells. The present research findings offer a new approach to achieve low-cost and high-efficiency solar cells.

Competing interests

The authors declare that they have no competing interests.

Authors' contributions

CC carried out the experiments, participated in the sequence alignment, and drafted the manuscript. FL participated in the device preparation. FW and FT participated in the design of the study. CL and YZ performed the statistical analysis. WZ conceived of the study and helped to draft the manuscript. All authors read and approved the final manuscript.

Author details

[1]School of Physics and Electronics, Henan University, Kaifeng 475004, People's Republic of China. [2]People's Republic of China and Henan Key Laboratory of Photovoltaic Materials, Henan University, Kaifeng 475004, People's Republic of China. [3]Institute of Modern Physics and School of Science, Huzhou Normal University, Huzhou 313000, People's Republic of China.

References

1. Suryawanshi MP, Agawane GL, Bhosale SM, Shin SW, Patil PS, Kim JH, Moholkar AV: **CZTS based thin film solar cells: a status review.** *Mater Technol* 2013, **28**:98–109.
2. Barkhouse DAR, Gunawan O, Gokmen T, Todorov TK, Mitzi DB: **Device characteristics of a 10.1% hydrazine-processed Cu2ZnSn(Se, S)4 solar cell.** *Prog Photovolt Res Appl* 2012, **20**:6–11.
3. Greätzel M, Janssen RAJ, Mitzi DB, Sargent EH: **Materials interface engineering for solution-processed photovoltaics.** *Nature* 2012, **488**:304–312.
4. Chang LY, Lunt RR, Brown PR, Bulovic V, Bawendi MG: **Low-temperature solution-processed solar cells based on PbS colloidal quantum Dot/CdS heterojunctions.** *Nano Lett* 2013, **1**:994–999.
5. Rath AK, Bernechea M, Martinez L, de Arquer FPG, Osmond J, Konstantatos G: **Solution-processed inorganic bulk nano-heterojunctions and their application to solar cells.** *Nat Photonics* 2012, **6**:529–534.
6. Tian YY, Zhang YJ, Lin YZ, Gao K, Zhang YP, Liu KY, Yang QQ, Zhou X, Qin DH, Wu HB, Xia YX, Hou LT, Lan LF, Chen JW, Wang D, Yao RH: **Solution-processed efficient CdTe nanocrystal/CBD-CdS hetero-junction solar cells with ZnO interlayer.** *J Nanopart Res* 2013, **15**:2053.
7. Gur I, Fromer NA, Geier ML, Alivisatos AP: **Air-stable all-inorganic nanocrystal solar cells processed from solution.** *Science* 2005, **310**:462–465.
8. Gur I, Fromer NA, Chen CP, Kanaras AG, Alivisatos AP: **Hybrid solar cells with prescribed nanoscale morphologies based on hyperbranched semiconductor nanocrystals.** *Nano Lett* 2007, **7**:409–414.
9. Azimi H, Heumuller T, Gerl A, Matt G, Kubis P, Distaso M, Ahmad R, Akdas T, Richter M, Peukert W, Brabec CJ: **Relation of nanostructure and recombination dynamics in a Low-temperature solution-processed CuInS$_2$ nanocrystalline solar cell.** *Adv Energ Mater* 2013, **3**:1589–1596.
10. Li L, Coates N, Moses D: **Solution-processed inorganic solar cell based on in situ synthesis and film deposition of CuInS$_2$ nanocrystals.** *J Am Chem Soc* 2010, **132**:22–23.
11. Todorov T, Sugimoto H, Gunawan O, Gokmen T, Mitzi DB: **High-efficiency devices with pure solution-processed Cu2ZnSn(S, Se) (4) absorbers.** *IEEE J Photovolt* 2014, **4**:483–485.
12. Hodes G: **Perovskite-based solar cells.** *Science* 2013, **342**:317–318.
13. Xing GC, Mathews N, Sun SY, Lim SS, Lam YM, Grätzel M, Mhaisalkar S, Sum TC: **Long-range balanced electron- and hole-transport lengths in organic–inorganic CH$_3$NH$_3$PbI$_3$.** *Science* 2013, **342**:344–347.
14. Stranks SD, Eperon GE, Grancini G, Menelaou C, Alcocer MJP, Leijtens T, Herz LM, Petrozza A, Snaith HJ: **Electron–hole diffusion lengths exceeding 1 micrometer in an organometal trihalide perovskite absorber.** *Science* 2013, **342**:341–344.
15. Kim HS, Lee CR, Im JH, Lee KB, Moehl T, Marchioro A, Moon SJ, Humphry-Baker R, Yum JH, Moser JE, Grätzel M, Park NG: **Lead iodide perovskite sensitized all-solid-state submicron thin film mesoscopic solar cell with efficiency exceeding 9%.** *Sci Rep UK* 2012, **2**:591.
16. Lee MM, Teuscher J, Miyasaka T, Murakami TN, Snaith HJ: **Efficient hybrid solar cells based on meso-superstructured organometal halide perovskites.** *Science* 2012, **338**:643–647.
17. Burschka J, Pellet N, Moon S-J, Humphry-Baker R, Gao P, Nazeeruddin MK, Grätzel M: **Sequential deposition as a route to high-performance perovskite-sensitized solar cells.** *Nature* 2013, **499**:316–319.
18. Heo JH, Im SH, Noh JH, Mandal TN, Lim CS, Chang JA, Lee YH, Kim HJ, Sarkar A, Nazeeruddin MK, Grätzel M, Seok SI: **Efficient inorganic–organic hybrid heterojunction solar cells containing perovskite compound and polymeric hole conductors.** *Nat Photonics* 2013, **7**:487–492.
19. Abrusci A, Stranks SD, Docampo P, Yip HL, Jen AKY, Snaith HJ: **High-performance perovskite-polymer hybrid solar cells via electronic coupling with fullerene monolayers.** *Nano Lett* 2013, **13**:3124–3128.
20. Park NG: **Organometal perovskite light absorbers toward a 20% efficiency low-cost solid-state mesoscopic solar cell.** *J Phys Chem Lett* 2013, **4**:2423–2429.
21. Liu MZ, Johnston MB, Snaith HJ: **Efficient planar heterojunction perovskite solar cells by vapour deposition.** *Nature* 2013, **501**:395–398.
22. Etgar L, Gao P, Xue ZS, Peng Q, Chandiran AK, Liu B, Nazeeruddin MK, Grätzel M: **Mesoscopic CH$_3$NH$_3$PbI$_3$/TiO$_2$ heterojunction solar cells.** *J Am Chem Soc* 2012, **134**:17396–17399.
23. Ball JM, Lee MM, Hey A, Snaith HJ: **Low-temperature processed meso-superstructured to thin-film perovskite solar cells.** *Energ Environ Sci* 2013, **6**:1739–1743.
24. Carnie MJ, Charbonneau C, Davies ML, Troughton J, Watson TM, Wojciechowski K, Snaith H, Worsley DA: **A one-step low temperature processing route for organolead halide perovskite solar cells.** *Chem Commun* 2013, **49**:7893–7895.
25. Kumar MH, Yantara N, Dharani S, Grätzel M, Mhaisalkar S, Boix PP, Mathews N: **Flexible, low-temperature, solution processed ZnO-based perovskite solid state solar cells.** *Chem Commun (Camb)* 2013, **49**:11089–11091.
26. Chung I, Lee B, He JQ, Chang RPH, Kanatzidis MG: **All-solid-state dye-sensitized solar cells with high efficiency.** *Nature* 2012, **485**:U486–U494.
27. Tell B, Shay JL, Kasper HM: **Electrical properties, optical properties, and band structure of CuGaS$_2$ and CuInS$_2$.** *Phys Rev Biol* 1971, **4**:2463–2471.
28. Li TL, Teng HS: **Solution synthesis of high-quality CuInS$_2$ quantum dots as sensitizers for TiO$_2$ photoelectrodes.** *J Mater Chem* 2010, **20**:3656–3664.
29. Shi L, Yin PQ, Wang LB, Qian YT: **Fabrication of single-crystalline CuInS$_2$ nanowires array via a diethylenetriamine-thermal route.** *Crystengcomm* 2012, **14**:7217–7221.
30. Baikie T, Fang YN, Kadro JM, Schreyer M, Wei FX, Mhaisalkar SG, Grätzel M, White TJ: **Synthesis and crystal chemistry of the hybrid perovskite (CH$_3$NH$_3$) PbI$_3$ for solid-state sensitised solar cell applications.** *J Mater Chem A* 2013, **1**:5628–5641.
31. Zhou ZJ, Fan JQ, Wang X, Sun WZ, Zhou WH, Du ZL, Wu SX: **Solution fabrication and photoelectrical properties of CuInS$_2$ nanocrystals on TiO$_2$ nanorod array.** *Acs Appl Mater Interfaces* 2011, **3**:2189–2194.
32. Chen C, Ali G, Yoo SH, Kum JM, Cho SO: **Improved conversion efficiency of CdS quantum dot-sensitized TiO$_2$ nanotube-arrays using CuInS$_2$ as a co-sensitizer and an energy barrier layer.** *J Mater Chem* 2011, **21**:16430–16435.
33. Im J-H, Lee C-R, Lee J-W, Park S-W, Park N-G: **6.5% efficient perovskite quantum-dot-sensitized solar cell.** *Nanoscale* 2011, **3**:4088–4093.
34. Na SI, Kim TS, Oh SH, Kim J, Kim SS, Kim DY: **Enhanced performance of inverted polymer solar cells with cathode interfacial tuning via water-soluble polyfluorenes.** *Appl Phys Lett* 2010, **97**:223305.
35. Belghachi A: **Perimeter recombination in thin film solar cells.** *J Comput Electron* 2007, **6**:279–283.

36. Kim HS, Lee JW, Yantara N, Boix PP, Kulkarni SA, Mhaisalkar S, Gräetzel M, Park NG: **High efficiency solid-state sensitized solar cell-based on submicrometer rutile TiO$_2$ nanorod and CH$_3$NH$_3$PbI$_3$ perovskite sensitizer.** *Nano Lett* 2013, **13**:2412–2417.
37. Jeng JY, Chiang YF, Lee MH, Peng SR, Guo TF, Chen P, Wen TC: **CH$_3$NH$_3$PbI$_3$ perovskite/fullerene planar-heterojunction hybrid solar cells.** *Adv Mater* 2013, **25**:3727–3732.